A quantum cascade laser cw cavity ringdown spectrometer coupled to a supersonic expansion source

Brian E. Brumfield,[1] Jacob T. Stewart,[1] Susanna L. Widicus Weaver,[1,a)]
Matthew D. Escarra,[2] Scott S. Howard,[2,b)] Claire F. Gmachl,[2] and Benjamin J. McCall[3]
[1]*Department of Chemistry, University of Illinois, Urbana, Illinois 61801, USA*
[2]*Department of Electrical Engineering, Princeton University, Princeton, New Jersey 08544, USA*
[3]*Departments of Chemistry and Astronomy, University of Illinois, Urbana, Illinois 61801, USA*

(Received 1 December 2009; accepted 19 April 2010; published online 8 June 2010)

A new instrument has been constructed that couples a supersonic expansion source to a continuous wave cavity ringdown spectrometer using a Fabry–Perot quantum cascade laser (QCL). The purpose of the instrument is to enable the acquisition of a cold, rotationally resolved gas phase spectrum of buckminsterfullerene (C_{60}). As a first test of the system, high resolution spectra of the ν_8 vibrational band of CH_2Br_2 have been acquired at $\sim$1197 cm^{-1}. To our knowledge, this is the first time that a vibrational band not previously recorded with rotational resolution has been acquired with a QCL-based ringdown spectrometer. 62 transitions of the three isotopologues of CH_2Br_2 were assigned and fit to effective Hamiltonians with a standard deviation of 14 MHz, which is smaller than the laser frequency step size. The spectra have a noise equivalent absorption coefficient of 1.4×10^{-8} cm^{-1}. Spectral simulations of the band indicate that the supersonic source produces rotationally cold ($\sim$7 K) molecules. © *2010 American Institute of Physics.*
[doi:10.1063/1.3427357]

I. INTRODUCTION

High resolution midinfrared (mid-IR) absorption spectroscopy has long been used as a sensitive tool for studying the fundamental bands of vibrational modes in polyatomic molecules. These modes serve as a molecule's "fingerprints," which not only provide important information about a molecule's structure and dynamics, but can also be used to detect its presence in nonlaboratory environments, including astronomical objects. Mid-IR spectroscopy is particularly valuable for studying symmetric molecules that lack permanent dipole moments and therefore cannot be studied using pure rotational spectroscopy. Examples of symmetric molecules that have been detected in astronomical objects based on high-resolution mid-IR laboratory spectroscopy include H_3^+,[1] C_2H_2,[2] CH_4,[3] and C_6H_6.[4]

The present study is motivated by the desire to search for C_{60}, which was serendipitously discovered in the laboratory during experiments designed to understand carbon star outflow chemistry[5] in astronomical environments. Of the four infrared active modes of C_{60}, only the mode near 1185 cm^{-1} is accessible for ground-based astronomical spectroscopy, as it lies in a region where the atmosphere is relatively transparent. The two major challenges in acquiring a rotationally resolved laboratory spectrum of C_{60} are developing a spectrometer with very high resolution and sensitivity near 8.5 μm, and preparing a sample of cold C_{60} in the gas phase. It should be noted that similar challenges apply to the spectroscopy of other large and symmetric carbon-bearing molecules, such as other fullerenes and polycyclic aromatic hydrocarbons. These challenges can be overcome with instruments constructed using sensitive laser direct absorption techniques coupled with high-temperature supersonic expansion sources.

Historically, there have been pulsed, and a lesser number of continuous wave (cw), laser sources available in the 8 μm region, but fewer than available in the visible and near-IR regions of the electromagnetic spectrum. Light sources such as cw optical parametric oscillators and difference frequency generation systems based on periodically poled lithium niobate (PPLN) crystals are capable of generating light spanning 2–5 μm, but progress of cw nonlinear light generation >5 μm has yet to mature to the point of offering performance comparable to those of current systems based on PPLN technology.[6] CO and CO_2 molecular gas lasers only offer partial frequency coverage from 5–6 μm and 9–11 μm, respectively.[6] Lead salt diode lasers are available in the mid-IR, but their narrow frequency coverage has limited their application.

However, the advent of quantum cascade lasers (QCLs) has enabled the fabrication of lasers with center frequencies spanning a large wavelength region in the mid-IR, using standard semiconductor materials. This is possible because the thickness of the semiconductor layers, and not their intrinsic band gap, can be varied to control the emitted photon energy.[7] Whereas lead salt diode lasers tend to have poor beam quality, generally low output powers (<1 mW), and require cryogenic cooling,[6,8] QCLs are now available with near-Gaussian beam output profiles, tens or hundreds of milliwatts of output power, and the capability to operate at room temperature. In addition to these favorable characteristics, free-running QCLs have short-term (<1 s) linewidths of

a)Present address: Department of Chemistry, Emory University, Atlanta, Georgia 30322, USA.
b)Present address: School of Applied and Engineering Physics, Cornell University, Ithaca, New York 14853, USA.

~1 MHz,[9] and submegahertz linewidths when actively frequency stabilized.[10] In comparison to nonlinear light generation methods, QCLs provide narrow spectral coverage (~20 cm^{-1}), but the development of external cavity systems and fabricated QCL arrays (providing broad coverage up to ~300 cm^{-1}) are now overcoming this difficulty.[11–13]

Consequently, QCLs are emerging as an attractive option for performing high resolution spectroscopy in the mid-IR, and have been successfully implemented into a variety of spectrometers utilizing wavelength modulation,[14–17] frequency modulation,[18] sub-Doppler Lamb dip spectroscopy,[15,19,20] integrated cavity output spectroscopy,[21–25] cw cavity ringdown spectroscopy (cw-CRDS),[26,27] and noise immune cavity enhanced optical heterodyne spectroscopy.[28] A majority of these studies were motivated as proof-of-concept implementations of cw-QCLs into previously existing techniques and/or for trace gas sensing pertinent to atmospheric science, biomedical breath analysis, and pollutant monitoring. However, two studies using QCL-based spectrometers have been carried out where a pulsed supersonic expansion was used to collect rotationally cold spectra of large molecules.[25,29]

As mentioned above, the second challenge for spectroscopy of C_{60} or related molecules is the preparation of a sample of rotationally cold gas-phase molecules. The use of supersonic expansions for cooling large molecules is a fairly mature science.[30,31] For large organic molecules, laser ablation/desorption and direct heating have been used to introduce the sample into supersonic expansions.[30–35] Using cw-CRDS with laser ablation adds the additional complication of timing the occurrence of ringdown events with the presence of sample in the supersonic jet. Though coupling cw-CRDS to pulsed sample delivery/generation has been achieved before,[36,37] given the thermal stability of C_{60} against decomposition, it is more straightforward to heat the C_{60} sample to high temperatures to provide a continuous feed of gas phase C_{60}. The high temperatures necessary to generate a significant C_{60} vapor pressure preclude the use of a pulsed supersonic expansion source, and requires a high-throughput pumping system to handle the gas load of a cw supersonic expansion source.

In the following sections, we present the experimental design and implementation of our QCL-based cw cavity ringdown spectrometer. We then present the results of our spectroscopy of a test molecule, methylene bromide (CH_2Br_2), which demonstrates the high resolution and sensitivity of our spectrometer, as well as the effectiveness of our supersonic expansion source when operated at room temperature.

II. EXPERIMENTAL

An overview of the apparatus is presented in Fig. 1. The system can be broken down into four principal parts: the quantum cascade laser (and its associated control electronics and housing), the optical layout, the data acquisition system, and the supersonic expansion source; each is described in detail below.

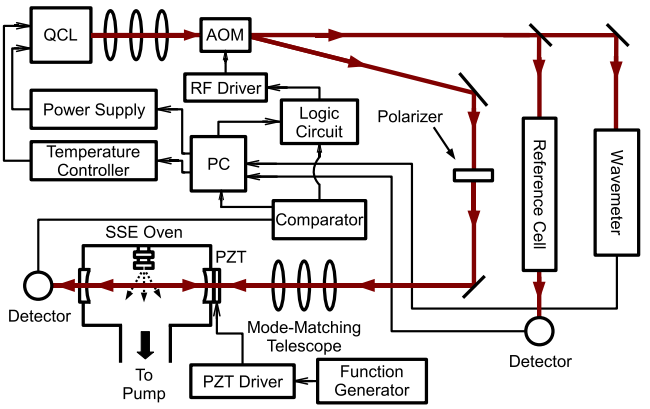

FIG. 1. (Color online) Overall experimental layout of the FP-QCL CRD spectrometer.

A. QCL

The QCLs used in the instrument have been designed and fabricated for this experiment at Princeton, with an active region design similar to that used for previously described 8.2 μm devices.[38] Unlike QCLs employing distributed feedback gratings, the lasers used in this study have short Fabry–Perot cavity lengths of ~2 mm to reduce multimode emission at higher currents (~700 mA). This approach removes the complication of adding a grating to the device, while increasing the yield of devices with the desired wavelength coverage. Shorter cavity lengths lead to a trade-off in power since the gain medium length is reduced, but there is still ample power with the shorter cavity design to carry out cavity ringdown spectroscopy.

The laser is housed inside a liquid nitrogen cooled cryostat. The cryostat was originally an unmodified Janis VPF-100, but this configuration had issues with a gradual drift in the laser pointing, and the cryostat reservoir only provided enough coolant to run for 1 h at a time. Because of these issues, significant modifications were made to the cryostat configuration.

To stabilize the laser pointing, a rigid armature was constructed, as shown in Fig. 2, and was mounted in place of one of the four cryostat windows. The copper sample mount was then disconnected from the cryostat cold plate, and held by the armature through compression of washers (outer diameter 0.25 in., inner diameter 0.115 in., thickness 0.115 in.) made of garolite (G10), a very low thermal conductivity material.[39] This was necessary to maintain reasonable thermal isolation between the cryostat outer shell and the copper submount. Thermal contact with the cold bath was achieved using a series of folded copper ribbons between the copper laser mount and the cold plate. The addition of an armature eliminated the drifting in the laser beam pointing, but because of the reduced cross-sectional area of the copper ribbons compared to the original mounting arrangement, the lowest achievable temperature with the laser operating is ~106 K. This issue has been addressed before with a different type of flexible thermal connection.[25]

In addition to the armature, the VPF-100 internal body was exchanged for a Janis Supertran FHT-ST internal body, which accepts a transfer line allowing a continuous flow of

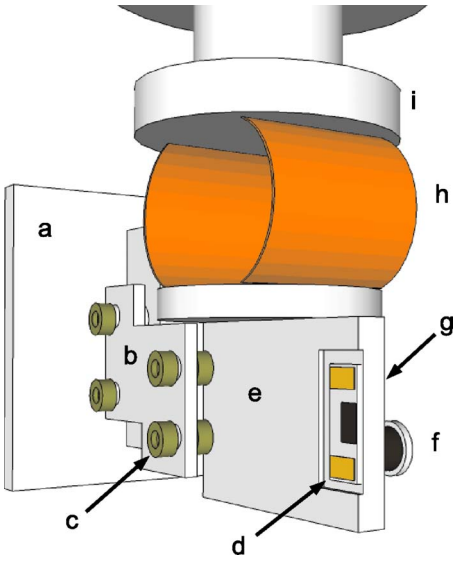

FIG. 2. (Color online) Schematic of rigid armature mount designed to eliminate laser drift as the cryostat liquid nitrogen level changed. (a) Back mounting plate; (b) armature; (c) G10 washer; (d) QCL chip; (e) copper laser mount; (f) resistive heater; (g) temperature diode (hidden from view, but adjacent to resistive heater on backside of mount); (h) copper ribbon; (i) cryostat cold plate.

liquid nitrogen to be delivered to cool the laser. This eliminated the need to refill a liquid nitrogen reservoir in hourly intervals. The liquid nitrogen is provided by an 80 L self-pressurizing liquid nitrogen Dewar (Cryofab CLPB 80-VW), which is capable of providing more than 40 h of laser run time between Dewar refills.

The laser current is provided by an ILX Lightwave (LDX-3232) power supply. To prevent inadvertent application of the wrong polarity of the applied current (which destroys the laser), a Zener diode has been added between the power supply and the laser. Additionally, the computer interface program has a high current limit that prevents a user from inadvertently applying dangerously high currents (>825 mA) to the laser. Even if this fail-safe were compromised, a built-in hardware current limit has been set on the power supply.

A Lakeshore (Model 341S) temperature controller is used in conjunction with a silicon temperature diode and a resistive heater to stabilize the temperature of the copper mount holding the QCL. The positioning of the heater and temperature sensor are shown in Fig. 2. The silicon temperature diode is positioned on the bottom of the copper mount opposite the side where the QCL is mounted, and the resistive heater is positioned adjacent to the diode on the same side of the mount. The long-term temperature stability ($\geqslant 1$ s) maintained using this configuration is $\Delta T \sim \pm 0.005$ K, as estimated by the measured laser frequency jitter using the Bristol mid-IR wavemeter and the temperature-to-frequency relationship for the laser.

To protect against accidental laser operation at temperatures that would damage the laser (>160 K), the laser current is routed through a relay in the temperature controller. The relay is programmed to close only after the cryostat temperature dips below 90 K, and to open if the laser temperature exceeds 160 K, thus preventing operation of the laser when the liquid nitrogen has run out in the self-pressurizing Dewar.

Laser frequency tuning is carried out by manipulating both the laser current start point and the temperature of the submount. By increasing the laser core temperature, either by increasing the laser current or the temperature of the laser mount, the laser output is downshifted in frequency. From empirical observations the laser has a frequency-to-current conversion of ~ 8 cm^{-1}/A, and a frequency-to-temperature conversion of ~ 0.08 cm^{-1}/K.

Using a variety of temperature and current conditions, it is possible to tune the laser in regions between 1183 and 1201 cm^{-1}. Complete coverage of the 18 cm^{-1} frequency span is not achieved due to laser mode-hops. The position of the mode-hops and tuning regions where the laser is stable can vary after an optical alignment. In regions where the laser can scan, it is possible to cover up to ~ 1 cm^{-1} before a mode-hop.

The frequency output of the QCL depends strongly on the temperature of the submount (and therefore the laser) when the laser current is brought above threshold. By monitoring the frequency output of the QCL using a cw wavemeter (Bristol 621B), it is possible to map out these temperature regions, allowing one to reproducibly bring the laser above threshold at a desired output frequency. The conditions for adjusting the laser output around 1185 cm^{-1} (C_{60}) and 1197 cm^{-1} (CH_2Br_2) can be determined through trial and error for a given optical alignment.

B. Optical layout

The divergent light output from the QCL passes through an antireflective (AR)-coated 3 in. diameter ZnSe window on the cryostat and is collimated by a 1 in. diameter AR-coated ZnSe aspheric lens (fl=2.54 cm). Light exiting the sphere is sent to a two element telescope comprised of a plano-convex BaF_2 lens (fl=50 cm) and a biconvex BaF_2 lens (fl =6.35 cm). This produces a small diameter beam that is then passed through an acousto-optic modulator (AOM). By careful alignment of the orientation of the AOM (Modulator Isomet 1207B with rf driver RFA241), and adjustment of the applied rf power, it is possible to attain a first order deflection efficiency approaching 85%. The first order beam is captured and gradually refocused using another plano-convex BaF_2 lens (fl=50 cm), and used for ringdown spectroscopy; the zero order beam is used for reference measurements.

The QCL is extremely sensitive to optical feedback, leading to issues with both the frequency coverage and the amount of mode-hop free tuning coverage achieved. To get the laser to scan stably, two approaches were utilized. First, it was necessary to tilt all of the optical components in the beam path. Second, the first order beam was passed through a holographic wire grid polarizer (Thorlabs WP25H-B). During scanning the wire grid polarizer transmission axis was kept at 20°–45° with respect to the horizontal polarization of the laser beam, corresponding to losses of 10% to 50%. In this capacity the wire grid polarizer may have served as a variable attentuator, reducing the amount of power available

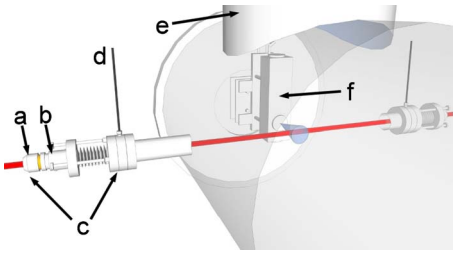

FIG. 3. (Color online) View of the chamber showing how the ringdown cavity axis is perpendicular to the expansion axis from the supersonic source. The vacuum chamber is rendered translucent in the figure. The laser beam is shown entering the mirror mount and crosses the free-jet (shown as a cone) emerging from the source. (a) Cavity ringdown mirror mount; (b) PZT; (c) kinematic mirror mount assembly; (d) N_2 purge gas line; (e) roots blower; (f) supersonic expansion source.

to back-reflect off the input ringdown mirror high reflectivity coating. The combination of these approaches reduced back reflections to the point where $\sim 1\ \mathrm{cm}^{-1}$ mode-hop free scanning is possible. A prototype optical isolator was also tested, but the amount of absorption from the optical isolator medium for a given amount of optical rotation made this approach unsuitable.

After passing through the polarizer, the first-order beam is coupled into the high finesse cavity using a three lens mode-matching telescope mounted on a meter-long dove-tail optics rail. This telescope facilitates mode-matching to the TEM_{00} mode of the ringdown cavity, and consists of a plano-convex BaF_2 (fl=20 cm), a biconcave CaF_2 (fl=−7.6 cm), and a plano-convex BaF_2 lens (fl=50 cm).

The ringdown cavity is formed from two $R(\lambda \sim 8.5\ \mu\mathrm{m}) > 0.9998$ mirrors (Laser Power Optics) with 6 m radius of curvature. The mirrors are held in homemade kinematic mounts with three precision screws to allow two-axis adjustment of their orientation. These mounts mate to ConFlat half-nipples that have been welded to the stainless steel vacuum chamber. The ringdown cavity axis is perpendicular to the supersonic expansion axis, as shown in Fig. 3. Between the vacuum chamber housing the source and the ringdown mirrors there are Swagelok connections for flowing N_2 purge gas at roughly 700 SCCM (SCCM denotes cubic centimeters per minute at STP) to protect the ringdown mirrors, and to bring the chamber up to ambient pressure without risk of particulates settling onto the mirror surfaces.

The ringdown mirror on the same side as the mode-matching telescope is mounted to a piezoelectric transducer (PZT) (Piezomechanik HPSt 150/20–15/25 VS-35) driven by a high voltage driver (Thorlabs MDT694A), with a sawtooth voltage waveform provided by a function generator. The voltage ramp applied to the PZT dithers the cavity resonances by more than one free spectral range to ensure that the laser frequency will come into resonance with the cavity at least twice during one PZT modulation cycle. Light leaking out of the cavity is focused by a short focal length plano-convex BaF_2 lens (fl=6.35 cm) onto a photoconductive mercury cadmium telluride detector (PC-MCT) (Infrared Associates MCT-9–1.0) with a 1 MHz preamplifier (Infrared Development Systems 1205). The noise equivalent power for the detector with the amplifier is $1.85 \times 10^{-12}\ \mathrm{W}/\sqrt{\mathrm{Hz}}$. The output from the MCT preamplifier is split to a high speed comparator and a 100 MHz 14-bit high speed digitizer card (National Instruments PCI-5122).

The reference arm of the optical layout relies on the zero order beam exiting the AOM. This beam is gradually refocused using a long focal length (98.7 cm) plano-convex CaF_2 lens. A ZnSe window is used as a beamsplitter, sending a small portion of the beam through a 45 cm long absorption cell, which is normally filled with SO_2 or N_2O. Light exiting the absorption cell is focused by an off-axis parabolic mirror (Janos fl=7.63 cm) onto a photovoltaic mercury zinc cadmium telluride detector (Vigo Technologies PVM-10.6) with a 1 MHz bandwidth preamplifier (VPDC-1S). The voltage output from the detector is connected to the input channel on a data acquisition board (National Instruments PCI-6221).

The remainder of the zero order beam is sent to a wavemeter. The QCL beam and the 50 μW red tracer beam from the wavemeter are initially made collinear over 1 m to align the QCL beam into the wavemeter. In this process, the QCL beam is visualized by observing the scattered mid-IR light on irises using a thermal infrared imaging camera (FLIR ThermaCam 320EX). The wavemeter has a specified accuracy of $0.001\ \mathrm{cm}^{-1}$ if it is properly aligned. However, good alignment produced a sufficient back reflection to promote laser mode-hops, and we therefore deliberately misalign the QCL beam such that the wavemeter reading is offset by $\sim 200-300$ MHz. To account for this, we calibrate the wavemeter reading using absorption lines in the direct absorption cell. The wavemeter therefore serves only as a relative frequency measurement tool, but also provides a lower accuracy real-time measure of the QCL frequency as the laser current and temperature are actively adjusted. The difference between the frequency of the first and zero order beams due to the Bragg downshifting of the first order beam is 40 MHz, and is accounted for during the frequency calibration procedure.

C. Data acquisition

During acquisition of a spectrum, the laser mount is held at a fixed temperature, while the current is stepped in small user-defined increments. The PZT is constantly dithered, bringing the ringdown cavity periodically in resonance with the laser, a scheme originally employed by Ref. 40. At each laser current, a number of ringdown transients are acquired and fit to exponential decays. Finally, direct absorption and wavemeter data are then acquired for frequency calibration. After the calibration data are collected, the laser current is then stepped. The data acquisition process is controlled by a personal computer (PC) running homemade LabWindows code, a comparator, and an AOM control circuit, as explained in more detail below.

The collection of each ringdown event begins when the cavity comes into resonance with the laser frequency, due to sweeping of the PZT, and the voltage output of the PC-MCT sharply increases. When this voltage reaches a user-defined threshold, the comparator sends out a transistor transistor logic (TTL) high pulse to the trigger input of the high speed

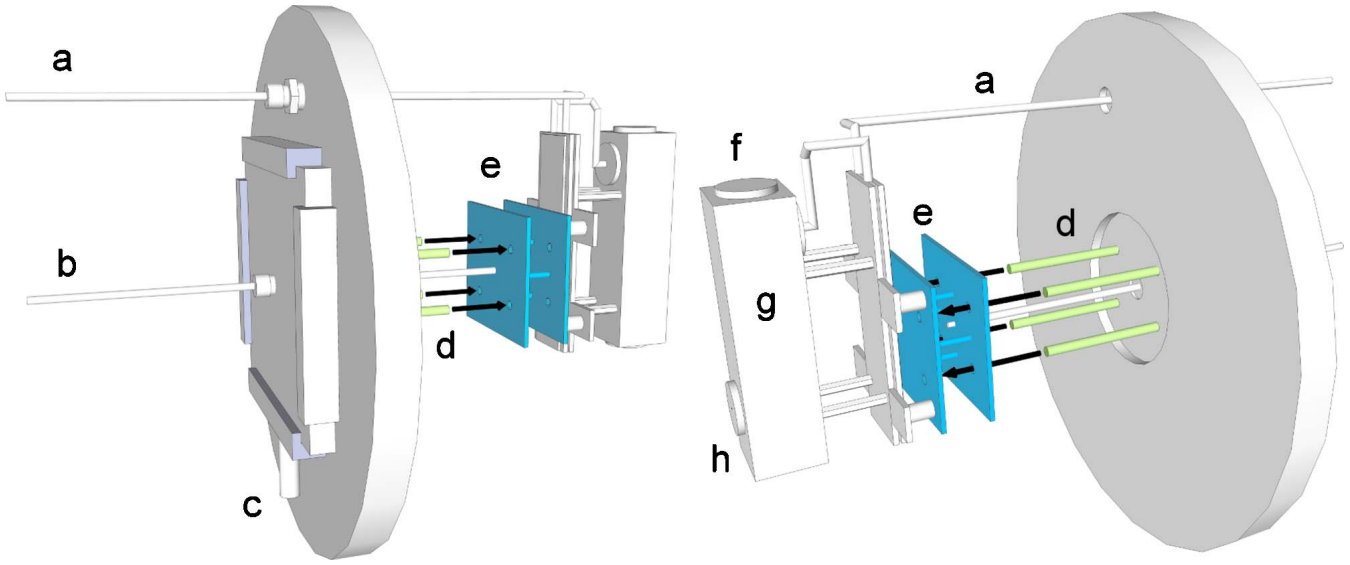

FIG. 4. (Color online) Two perspectives of the supersonic source mounted on a translatable plate attached to the back flange of the vacuum chamber. (a) Gas feedline to expansion source; (b) push-rod for adjusting nozzle distance from cavity axis; (c) height adjustment micrometer for the translatable plate; (d) rods for supporting source carriage; (e) source carriage plates; (f) Conflat blank used to seal source bore; (g) expansion source body; (h) pinhole nozzle machined into Conflat blank.

digitizer, and a TTL low pulse is sent to the AOM control circuit. The latter pulse triggers the AOM control circuit to output a TTL low pulse to the AOM rf driver, which removes the rf power from the AOM, suppressing the first order beam by −38 dB. The duration of this TTL low signal is a user set value on the comparator, and is adjusted so that one complete ringdown event can be collected without being spoiled by subsequent injection of light into the cavity. While the light going into the cavity is being attenuated, the TTL high pulse initiates data collection by the high speed digitizer. The decay event is fit in a data acquisition program using a fast algorithm that accommodates a nonzero baseline on the exponential decay.[41] Once the output time of the comparator TTL low signal has elapsed, the first order beam is turned on again, allowing the process of ringdown collection at a fixed laser current to continue.

Once the user defined number of ringdowns (typically 100) has been collected, a box-and-whiskers algorithm is used to remove the top and bottom quartile of the measured time constants. The remaining time constant values are then averaged, converted to an absorption coefficient, and recorded. The PC then sends a TTL high signal to the AOM control circuit, which overrides the signal sent from the comparator, and turns the AOM off for sufficient time to acquire calibration data. The intensity of light on the PC-MZCT detector (after passing through the direct absorption cell) is measured by the digital acquisition board, and the wavemeter is read through a universal serial bus interface. Also at this time, the laser current and temperature are read through a general purpose interface bus (GPIB) interface and recorded. Once the calibration data have been obtained, the LabWindows program uses the GPIB interface to step the laser current by a user-defined amount (typically 0.1 mA, which corresponds to ~23 MHz), and the data collection process starts again. This cycle continues until the laser current reaches the end of the desired scan range.

D. Supersonic expansion source and sample introduction

Figure 4 shows an overall view of the supersonic expansion source and its mounting in the vacuum chamber. The supersonic expansion source is composed of a stainless steel body with an attached pair of plates. The gas exits the oven body through a nozzle machined into a 1 1/3 in. ConFlat blank, which fits to a ConFlat "flange" machined into the source body (item h Fig. 4). This design makes it possible to test a variety of nozzle geometries by machining 1 1/3 in. Conflat blanks.

For the current methylene bromide jet studies a 700 μm pinhole nozzle was used. Slit nozzles were also available but not used. The slit nozzle would provide a reduction in linewidth in comparison to a pinhole nozzle,[42,43] and would provide a higher signal-to-noise (S/N) ratio for the transitions observed, but this increase is limited by the 30 MHz (0.001 cm^{-1}) linewidth of the laser. When carrying out C_{60} spectroscopy a slit nozzle geometry may be preferable because it affords better vibrational cooling due to an increase in the number of collisions early in the expansion, but this will come at the expense of an increased rotational temperature in comparison to a pinhole nozzle.[44] For flexibility it is preferable to have both nozzle types when the instrument will be used for C_{60} spectroscopy.

The source body is mounted to a carriage with two plates held in parallel (item e in Fig. 4). The parallel plates have four through-holes that line up with four rods extending from a *x*-*y* translatable flange on the back of the vacuum chamber (item d in Fig. 4). A rod is attached to the carriage and exits the chamber through an Ultra-Torr connection on the back flange (item b in Fig. 4); this allows the entire source assembly to be translated perpendicular to the ringdown cavity axis, thereby controlling the distance from the nozzle where the expansion is probed spectroscopically. The *x*-*y* translat-

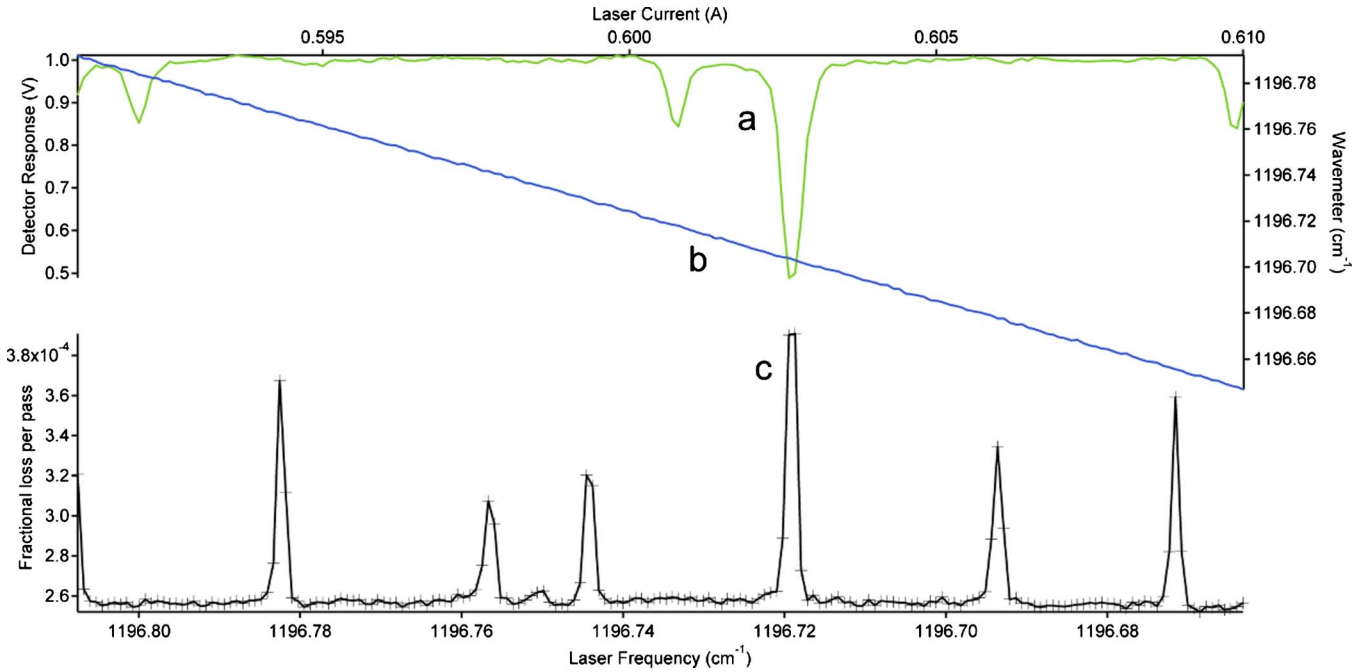

FIG. 5. (Color online) Example CH_2Br_2 scanning window of room temperature gas leaked into the chamber from 1196.792–1196.647 cm^{-1}. (a) Direct absorption scan (normalized) of SO_2. (b) Frequency readings from calibrated wavemeter. (c) Cavity ringdown spectrum of CH_2Br_2.

able flange allows adjustment of the vertical offset between the expansion and the cavity axis through the adjustment of a micrometer (item c in Fig. 4) that pushes against the translatable flange.

The supersonic source is backed by gas delivered from a mixing manifold constructed from four mass flow controllers (MKS M100B and 247D). One of the flow controllers is backed by Ar (S.J. Smith 99.95% purity) that is bubbled through methylene bromide (Aldrich 99% purity), while a second flow controller is backed with only Ar. The mole fraction of methylene bromide seeded in the expansion can then be adjusted by adjusting these two flow controllers.

While the mixing manifold and bubbler are useful for the introduction of methylene bromide to the source, the C_{60} sample introduction will be carried out differently. The C_{60} sample can be loaded directly into the hollow source bore (covered by the conflat blank labeled f in Fig. 4), which is accessible via another 1 1/3 in. ConFlat. The solid sample can be loaded in pellets that are held in place by sitting on top of a plug of quartz wool, separating the sample from the region of the bore just before the nozzle exit.

The extreme source temperatures when attempting C_{60} spectroscopy make it impractical to implement a pulsed supersonic expansion source. The large gas load generated by operating the source continuously is handled by a two-stage pumping system composed of a roots blower (Oerlikon-Leybold WS2001) and a rotary vane pump (Oerlikon-Leybold SV630). During normal flow conditions, with ~ 1 atm pressure measured after the flow controllers, and N_2 curtain gas flowing over the ringdown mirrors, the typical chamber background pressure is $\sim 20-40$ mTorr (~ 700 SCCM N_2 flow rate).

III. RESULTS AND DISCUSSION

A. Ringdown spectrometer performance

The performance of the spectrometer and the supersonic expansion source (operated at room temperature) have been evaluated using the ν_8 band of methylene bromide. Methylene bromide was selected as a test molecule because it has a vibrational band falling within the frequency coverage of our QCL. Several other molecules were considered, but methylene bromide has the advantages of being small (only five atoms), being commercially available, and whose mass is dominated by two heavy atoms making it a near prolate top with small rotational constants. The latter characteristics combine to make the rovibrational structure of the band simple, but also compact, so that it is not necessary to scan over a broad spectral window in order to estimate the rotational temperature in the expansion.

Figure 5 provides an example of one scanning window covering 0.15 cm^{-1} of the CH_2Br_2 vibrational band. This spectrum is not of a jet-cooled sample. The methylene bromide in this scan was leaked into the chamber through an open 0.25 in. inner diameter tube. Using the calibration traces, the maximum full width at half maximum (FWHM) of the spectral features seen in trace (c) is estimated to be 0.0013 cm^{-1} (40 MHz). Assuming a 30 MHz instrument linewidth, the estimated linewidth for the transition is ~ 30 MHz, which compares favorably with the 0.0011 cm^{-1} (33 MHz) FWHM Doppler broadening for a single methylene bromide line at room temperature. Between the spectral features the baseline standard deviation in the absorption coefficient is $\sim 1.4 \times 10^{-8}$ cm^{-1}, and represents the typical noise level of the system. Many spectra covering short frequency spans have been collected providing coverage from 1195.4 to 1197.15 cm^{-1}.

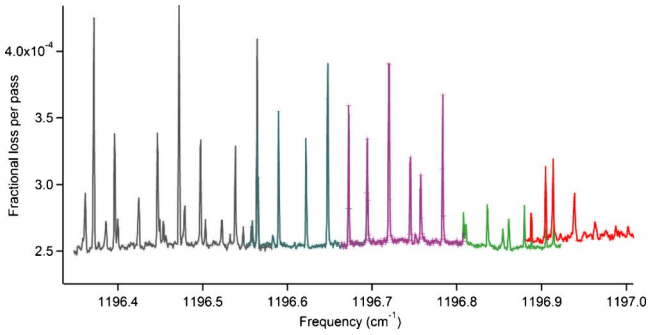

FIG. 6. (Color online) Collection of calibrated overlapped CH_2Br_2 spectra from 1196.5 to 1197.0 cm^{-1} illustrating the prominence of the strong Q-branch features from all three isotopologues. All these spectra are of room temperature gas that has been leaked into the chamber.

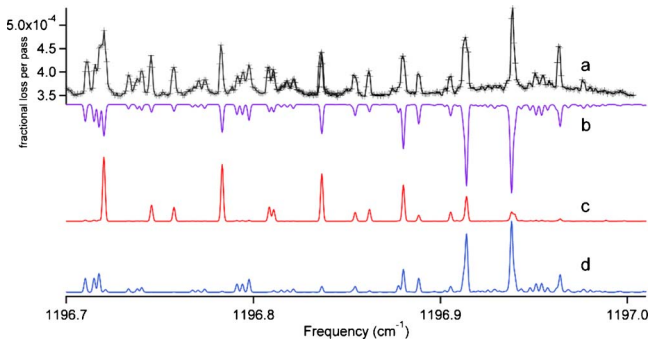

FIG. 7. (Color online) Comparison between recorded experimental spectra of CH_2Br_2 and simulated spectra with all three isotopologues at two different rotational temperatures. (a) Experimental spectra from 1196.50 to 1197.00 cm^{-1} with the nozzle 2.5 cm from the region probed, with the flow rates of the Ar only and Ar/CH_2Br_2 set to 660 and 102 SCCM, respectively; (b) simulated spectrum composed of a linearly scaled coaddition from simulations (c) and (d); (c) simulated spectrum at $T_{rot}=7$ K with a Gaussian linewidth of 0.0015 cm^{-1}; (d) simulated spectrum at $T_{rot}=300$ K with a Gaussian linewidth of 0.0015 cm^{-1}.

This is the first time that the ν_8 band of methylene bromide has been observed with sufficient resolution to reveal the rotational structure; previous spectra in the literature were acquired at low resolution, showing only the band contours of the P, Q, and R branches.[45,46] In order to evaluate the rotational cooling in the expansion, it was necessary to assign the high resolution spectrum of the jet-cooled sample.

Methylene bromide is a near-prolate asymmetric top with a Ray's asymmetry parameter of $\simeq -0.996$.[47] The CH_2 wagging motion of the ν_8 band results in a change of the dipole moment predominantly along the molecular *a*-axis, giving a parallel band structure. This leads to an easily assignable band structure, but the high abundance of two bromine isotopes provides an additional complication. The natural abundance of the ^{79}Br and ^{81}Br isotopes is roughly 1:1, and with the presence of two bromine atoms in methylene bromide a 1:2:1 abundance of $CH_2{}^{79}Br_2$, $CH_2{}^{79}Br^{81}Br$, and $CH_2{}^{81}Br_2$ isotopologues is expected in the sample. Each isotopologue will have its own parallel band, with small differences in the vibrational band center positions and rotational constants.

The detailed assignment was carried out using PGOPHER, a spectral assignment and fitting software package.[48] Ground state rotational constants from microwave spectroscopy of the $CH_2{}^{79}Br_2$,[49] $CH_2{}^{81}Br_2$,[49] and $CH_2{}^{79}Br^{81}Br$ (Ref. 50) isotopologues were used for both the ground and vibrational excited states for the initial spectral prediction.

The first set of assignments involved a progression of strong sharp spectral features seen in the spectrum of room temperature methylene bromide leaked into the chamber, as shown in Fig. 6. These features represent a series of Q-branch progressions for all three of the isotopologues. A single feature is composed of a series of tightly packed unresolved transitions sharing the same upper and lower K_a values. Because the features are narrow and not resolvable, each Q-branch feature is assigned to a single $(\nu'=1,\ J'=K_a'',\ K_a'=K_a'',\ K_c'=1) \leftarrow (\nu''=0,\ J''=K_a'',K_a'',\ K_c''=0)$ transition. In the figure, a rough 1:2:1 intensity ratio can be seen because of the isotope abundance, with the strongest features in the sequence belonging to the $CH_2{}^{79}Br^{81}Br$ isotopologue. It is important to note that not all of the spectral windows displayed in the figure were carried out with the same mole fraction of methylene bromide, so the intensities between different scanning windows cannot be directly compared.

Using these initial assignments of the Q-branches for $CH_2{}^{79}Br^{81}Br$, the experimental spectrum was fit, allowing only the band origin ν_0 and the excited state rotational constant A' to vary, with all other rotational constants constrained to values determined through pure rotational microwave spectroscopy. The Q-branch pattern resulting from fitting to these $CH_2{}^{79}Br^{81}Br$ assignments was then shifted higher in frequency to match the Q-branch progression for $CH_2{}^{79}Br_2$, and lower in frequency to assign the heavier $CH_2{}^{81}Br_2$ isotopologue. Comparison of simulations generated from fitting of the Q-branch features to the experimental spectra then enabled assignment of low J'' P-branch lines seen in the jet-cooled spectra as shown in Fig. 7.

The final results of the assignment and fitting are presented in Table I. The largest average |observed-calculated| (Avg. |o-c|) achieved for fitting to Q and P-branch transitions was 0.000 45 cm^{-1} (14 MHz). Given that the spectral features are under-sampled, that the spectra were acquired taking 0.000 77 cm^{-1} (23 MHz) frequency steps, and that only six parameters were used to fit 62 transitions, we consider this average o-c to be acceptable.

While the line frequencies of the simulations clearly match those of the experimental spectra, the simulated relative intensities (assuming a single rotational temperature) fail to match the experimental spectra acquired in the free-jet. Figure 7 highlights this by presenting two simulated spectra at T_{rot} of 300 and 7 K, traces (c) and (d), respectively. Neither simulation is a good match to the experimental spectra shown in trace (a). However, trace (b), which is a scaled linear combination of traces (c) and (d), compares better to the relative intensities of the experimental spectrum.

These results indicate that the observed spectrum is due to a combination of room temperature and rotationally cooled CH_2Br_2. Close to the band center, the Q-branch features corresponding to low K_a are dominated by the jet-cooled sample, while the room temperature contribution is negligible. Farther from the band origin (higher values of K_a), the intensity of the Q-branch features are dominated by

TABLE I. Compilation of spectroscopic constants obtained by fitting experimental spectra for all three isotopologues using PGOPHER. Only ν_0 and A' were fit, with the 1σ uncertainties from the fit provided in parentheses next to the value. A'' is taken from microwave studies, and shown for comparison to A'. The rightmost columns provide the average observed minus calculated for the fit, and the number of assigned lines for each isotopologue, respectively. The B and C rotational constants for all three isotopologues are not provided in the table because they were constrained to their values from microwave studies.

	Band constants (cm^{-1})				
	ν_0	A''	A'	Avg.|o−c|(cm^{-1})	# Assg. Lines
$CH_2{}^{79}Br_2$	1196.983 63(99)	0.868 311	0.863 451 9(22)	0.000 35	20
$CH_2{}^{79}Br^{81}Br$	1196.957 97(12)	0.867 519	0.862 664 9(28)	0.000 45	22
$CH_2{}^{81}Br_2$	1196.932 06(12)	0.866 756	0.861 910 8(23)	0.000 44	20

the room temperature background gas. The strength of the contribution from the background is not surprising because a majority of the 75 cm path length probed is chamber background gas, while the jet comprises a much smaller amount of the pathlength.

Near the band center, the relative intensities of the Q-branch features ($K_a \leq 2$) and the low-J P-branch transitions are best described by a simulation with $T_{rot}=7$ K. This illustrates the effectiveness of the expansion source for producing rotationally cold molecules, at least when operated at room temperature. The strength of the Q-branch features near the band center also serves as a feedback signal to optimize alignment overlap between the pinhole expansion source and the ringdown cavity axis.

The FWHM of the jet-cooled methylene bromide features is estimated to be ~50–60 MHz. The estimated FWHM is broader than transitions associated with the room temperature background sample. The linewidth discrepancy between the jet and background features agrees with past studies in Ar free-jets in the mid-IR, showing that the Doppler broadening associated with the expansion is greater than the room temperature Doppler broadening.[51–56] Our observed jet-cooled linewidth is comparable to, but narrower than, that seen in those previous studies.[51–56]

B. Comparison to previous QCL ringdown spectrometers

Two previous cw cavity ringdown spectrometers have been reported using QCLs.[26,27] Table II compares their single-shot standard deviations in the time constant and absorption coefficient with ours. In the two previous studies these single-shot values were determined in an empty cavity while holding the laser at a fixed frequency. The single-shot information for the current study is estimated from the measured standard deviation in the absorption coefficient (σ_α) in collected room temperature methylene bromide spectra where there are no measurable spectral features, and from the average ringdown collection rate and time constant. Close investigation of the baseline regions used did not reveal periodic fringing, as seen in the CRD study by Kosterev *et al.*[27] Because the ringdown spectra are the result of using the box-and-whiskers algorithm, the unfiltered noise level is likely worse than estimated. The σ_α was calculated using the following formula[27]

$$\sigma_\alpha = \frac{\frac{\sigma_\tau}{\langle\tau\rangle}}{c\langle\tau\rangle}, \tag{1}$$

where $\langle\tau\rangle$ is the average time constant, and σ_τ is the standard deviation of the time constant.

With a knowledge of the σ_α, and the ringdown repetition rate (f_{rep}), it is possible to calculate the instrumental sensitivity (Sy) using the following expression:[57]

$$Sy = \frac{\sigma_\alpha}{\sqrt{f_{rep}}}. \tag{2}$$

The Sy of the current study is significantly higher than the prior studies. The high Sy is related to the poor performance of our PC-MCT detector. While recording ringdown events it was necessary to start the exponential fit ~14 μs after receiving the TTL high trigger because of the long response time of the PC-MCT. This wait reduces the S/N in the portion of the decay that can be fit to a single exponential, leading to an increase in σ_τ. The comparator level also had to be set to a high voltage threshold in a trade-off between recording ringdown events with a significantly high S/N to

TABLE II. Comparison of the performance of previously reported QCL cw ringdown spectrometers with that of the current instrument.

	$\langle\tau\rangle$ (μs)	$\sigma_\tau/\langle\tau\rangle$	σ_α (cm^{-1})	f_{rep} transients (Hz)	Sy (cm^{-1} $Hz^{-1/2}$)
Paldus *et al.* (Ref. 26)	0.949	2×10^{-3}	7.2×10^{-8}	600	2.98×10^{-9}
Kosterev *et al.* (Ref. 27)	3.48	2.2×10^{-3}	2.2×10^{-8}	1600	5.50×10^{-10}
This work	~10	$\sim4.7\times10^{-2}$	1.58×10^{-7}	10	5.06×10^{-8}

improve the σ_τ, at the cost of a reduced ringdown collection rate, further impacting the instrumental sensitivity.

The manufacturer indicated that the rise time for the PC-MCT detector should be from 1 to 2 μs, which is in stark contrast to what was seen experimentally. This performance issue could in principle be due to saturation from the large amount of power directed at the detector, to issues with the AOM response, or due to a flaw with the detector itself. The power reaching the PC-MCT was reduced by two orders of magnitude, and no improvement was seen in the response of the detector to a single ringdown event. The AOM response was explored by triggering the AOM while looking at both the reference detector and PC-MCT response. The reference detector responded in 1 μs to the switching off of the AOM, while the PC-MCT took nearly 10 μs to decay to the background level.

Given these results, a PV-MCT from Kolmar Technologies (KMPV11–1-J1/AC) with a postamplifier (KA100-E2) was recently purchased as a replacement detector. This PV-MCT eliminated the long trigger delay issue, making it possible to fit after a 2.5 ms delay. Preliminary tests in an empty cavity have provided a $\sigma_\tau/\langle\tau\rangle \leq 1\times10^{-2}$, and a ringdown collection rate $\gtrsim$50 Hz. The current noise level achieved with the detector does not appear limited by the -38 dB on/off modulation ratio of the AOM, but this effect is known to cause an increase in the noise level of a cw-CRD spectrometer.[58]

IV. CONCLUSIONS

The first high-resolution spectrum of the ν_8 band of methylene bromide has been collected using a quantum cascade laser based cw cavity ringdown spectrometer, coupled to a supersonic expansion source. To our knowledge, this represents the first time that a cw ringdown QCL spectrometer has been coupled with a supersonic free-jet for the purposes of spectral discovery. The high resolution of the spectrometer has allowed the assignment and fitting of the rovibrational bands for each isotopologue, which in turn has demonstrated the effectiveness of our supersonic expansion source for producing rotationally cold molecules. The methylene bromide spectrum can now be used as a tool to optimize the overlap between the supersonic expansion and the ringdown cavity when the oven is operating at room temperature.

ACKNOWLEDGMENTS

The authors wish to thank Richard Saykally for the loan of the cryostat and the cavity ringdown mirrors used in this work, and Frank Tittel for helpful conversations regarding the frequency stability of QCLs. We also wish to acknowledge experimental assistance from Brian Siller, Brian Pohrte, and Brett McGuire. The Illinois team acknowledges financial support from NASA Laboratory Astrophysics Grant No. NNG05GE59G, the Camille and Henry Dreyfus Foundation, the David and Lucile Packard Foundation, and the University of Illinois. The Princeton team has been supported by funding from the Mid-Infrared Technologies for Health and the Environment NSF Engineering Research Center.

[1] T. R. Geballe and T. Oka, Nature (London) **384**, 334 (1996).
[2] J. H. Lacy, N. J. Evans, J. M. Achtermann, D. E. Bruce, J. F. Arens, and J. S. Carr, Astrophys. J. **342**, L43 (1989).
[3] J. H. Lacy, J. S. Carr, N. J. Evans, F. Baas, J. M. Achtermann, and J. F. Arens, Astrophys. J. **376**, 556 (1991).
[4] J. Cernicharo, A. M. Heras, A. G. G. M. Tielens, J. R. Pardo, F. Herpin, M. Guelin, and L. B. F. M. Waters, Astrophys. J. Lett. **546**, L123 (2001).
[5] H. Kroto, J. Heath, S. Obrien, R. Curl, and R. Smalley, Nature (London) **318**, 162 (1985).
[6] A. Godard, C. R. Phys. **8**, 1100 (2007).
[7] F. Capasso, C. Gmachl, D. L. Sivco, and A. Y. Cho, Phys. Today **55**(5), 34 (2002).
[8] W. Tam, I. Leonov, and Y. Xu, Rev. Sci. Instrum. **77**, 063117 (2006).
[9] D. Weidmann, L. Joly, V. Parpillon, D. Courtois, Y. Bonetti, T. Aellen, M. Beck, J. Faist, and D. Hofstetter, Opt. Lett. **28**, 704 (2003).
[10] R. M. Williams, J. F. Kelly, J. S. Hartman, S. W. Sharpe, M. S. Taubman, J. L. Hall, F. Capasso, C. Gmachl, D. L. Sivco, J. N. Baillargeon, and A. Y. Cho, Opt. Lett. **24**, 1844 (1999).
[11] G. Wysocki, R. Lewicki, R. F. Curl, F. K. Tittel, L. Diehl, F. Capasso, M. Troccoli, G. Hofler, D. Bour, S. Corzine, R. Maulini, M. Giovannini, and J. Faist, Appl. Phys. B: Lasers Opt. **92**, 305 (2008).
[12] B. G. Lee, M. A. Belkin, R. Audet, J. MacArthur, L. Diehl, C. Pflugl, F. Capasso, D. C. Oakley, D. Chapman, A. Napoleone, D. Bour, S. Corzine, G. Höfler, and J. Faist, Appl. Phys. Lett. **91**, 231101 (2007).
[13] B. Lee, H. Zhang, C. Pflugl, L. Diehl, M. Belkin, M. Fischer, A. Wittmann, J. Faist, and F. Capasso, IEEE Photonics Technol. Lett. **21**, 914 (2009).
[14] W. Weber, J. Remillard, R. Chase, J. Richert, F. Capasso, C. Gmachl, A. Hutchinson, D. Sivco, J. Baillargeon, and A. Cho, Appl. Spectrosc. **56**, 706 (2002).
[15] A. Castrillo, E. De Tommasi, L. Gianfrani, L. Sirigu, and J. Faist, Opt. Lett. **31**, 3040 (2006).
[16] B. W. M. Moeskops, S. M. Cristescu, and F. J. M. Harren, Opt. Lett. **31**, 823 (2006).
[17] G. Hancock, J. H. van Helden, R. Peverall, G. A. D. Ritchie, and R. J. Walker, Appl. Phys. Lett. **94**, 201110 (2009).
[18] S. Borri, S. Bartalini, P. De Natale, M. Inguscio, C. Gmachl, F. Capasso, D. L. Sivco, and A. Y. Cho, Appl. Phys. B: Lasers Opt. **85**, 223 (2006).
[19] J. Remillard, D. Uy, W. Weber, F. Capasso, C. Gmachl, A. Hutchinson, D. Sivco, J. Baillargeon, and A. Cho, Opt. Express **7**, 243 (2000).
[20] N. Mukherjee and C. K. N. Patel, Chem. Phys. Lett. **462**, 10 (2008).
[21] Y. Bakhirkin, A. Kosterev, C. Roller, R. Curl, and F. Tittel, Appl. Opt. **43**, 2257 (2004).
[22] Y. Bakhirkin, A. Kosterev, R. Curl, F. Tittel, D. Yarekha, L. Hvozdara, M. Giovannini, and J. Faist, Appl. Phys. B: Lasers Opt. **82**, 149 (2006).
[23] M. R. McCurdy, Y. A. Bakhirkin, and F. K. Tittel, Appl. Phys. B: Lasers Opt. **85**, 445 (2006).
[24] M. R. McCurdy, Y. Bakhirkin, G. Wysocki, and F. K. Tittel, J. Biomed. Opt. **12**, 034034 (2007).
[25] Y. Xu, X. Liu, Z. Su, R. M. Kulkarni, W. S. Tam, C. Kang, I. Leonov, and L. D'Agostino, Proc. SPIE **7222**, 722208 (2009).
[26] B. Paldus, C. Harb, T. Spence, R. Zare, C. Gmachl, F. Capasso, D. Sivco, J. Baillargeon, A. Hutchinson, and A. Cho, Opt. Lett. **25**, 666 (2000).
[27] A. A. Kosterev, A. L. Malinovsky, F. K. Tittel, C. Gmachl, F. Capasso, D. L. Sivco, J. N. Baillargeon, A. L. Hutchinson, and A. Y. Cho, Appl. Opt. **40**, 5522 (2001).
[28] M. S. Taubman, T. L. Myers, B. D. Cannon, and R. M. Williams, Spectrochim. Acta, Part A **60**, 3457 (2004).
[29] J. F. Kelly, A. Maki, T. A. Blake, and R. L. Sams, J. Mol. Spectrosc. **252**, 81 (2008).
[30] A. Amirav, U. Even, and J. Jortner, Chem. Phys. **51**, 31 (1980).
[31] A. Amirav, U. Even, and J. Jortner, Chem. Phys. Lett. **83**, 1 (1981).
[32] J. R. Cable, M. J. Tubergen, and D. H. Levy, J. Am. Chem. Soc. **109**, 6198 (1987).
[33] N. A. van Dantzig, P. Piotrowiak, and D. H. Levy, Chem. Phys. Lett. **223**, 127 (1994).
[34] J. W. Elam and D. H. Levy, J. Phys. Chem. B **102**, 8113 (1998).
[35] L. C. Snoek, T. V. Mourik, and J. P. Simons, Mol. Phys. **101**, 1239 (2003).
[36] M. Hippler and M. Quack, Chem. Phys. Lett. **314**, 273 (1999).
[37] J. Thiébaud and C. Fittschen, Appl. Phys. B: Lasers Opt. **85**, 383 (2006).
[38] Z. Liu, D. Wasserman, S. Howard, A. Hoffman, C. Gmachl, X. Wang, T. Tanbun-Ek, L. Cheng, and F.-S. Choa, IEEE Photonics Technol. Lett. **18**, 1347 (2006).

[39] S. Acharya, F. Zhou, J. Lagrone, G. Mahmood, and R. S. Bunker, J. Turbomach. **127**, 471 (2005).
[40] D. Romanini, A. Kachanov, N. Sadeghi, and F. Stoeckel, Chem. Phys. Lett. **264**, 316 (1997).
[41] D. Halmer, G. von Basum, P. Hering, and M. Murtz, Rev. Sci. Instrum. **75**, 2187 (2004).
[42] K. Veeken and J. Reuss, Appl. Phys. B: Lasers Opt. **38**, 117 (1985).
[43] C. Lovejoy and D. Nesbitt, Rev. Sci. Instrum. **58**, 807 (1987).
[44] M. Sulkes, C. Jouvet, and S. A. Rice, Chem. Phys. Lett. **87**, 515 (1982).
[45] D. Bârcă-Gălăteănu, Z. Phys. **117**, 589 (1941).
[46] *Gases and Vapours*, edited by C. Craver (The Coblentz Society, Kirkwood, 1980).
[47] D. Chadwick and D. Millen, Trans. Faraday Soc. **67**, 1539 (1971).
[48] C. Western, PGOPHER, a program for simulating rotational structure, http://pgopher.chm.bris.ac.uk (2009).
[49] R. W. Davis and M. C. L. Gerry, J. Mol. Spectrosc. **109**, 269 (1985).
[50] Y. Niide, H. Tanaka, and I. Ohkoshi, J. Mol. Spectrosc. **139**, 11 (1990).
[51] G. M. Hansford, P. B. Davies, J. Gang, and D. K. Russell, Spectrochim. Acta, Part A **53**, 1755 (1997).
[52] J. Gang, M. Pennington, D. K. Russell, F. J. Basterrechea, P. B. Davies, and G. M. Hansford, J. Opt. Soc. Am. B **11**, 184 (1994).
[53] P. Asselin, P. Soulard, L. Manceron, V. Boudon, and G. Pierre, J. Mol. Struct. **517–518**, 145 (2000).
[54] P. B. Davies, G. M. Hansford, and T. C. Killian, J. Mol. Spectrosc. **163**, 138 (1994).
[55] P. R. Brown, P. B. Davies, G. M. Hansford, and N. A. Martin, J. Mol. Spectrosc. **158**, 468 (1993).
[56] K. S. Trauth, W. A. Burns, G. Berry, and S. W. Reeve, J. Chem. Phys. **120**, 4297 (2004).
[57] *Cavity-Ringdown Spectroscopy: An Ultratrace Absorption Measurement Technique*, edited by K. Busch and M. Busch (American Chemical Society, Washington, DC, 1999).
[58] H. Huang and K. Lehmann, Appl. Phys. B: Lasers Opt. **94**, 355 (2009).